Polar Polymeric Langmuir–Blodgett Films Containing Nitrobiphenyl Groups

S. H. Ou,† V. Percec,† J. A. Mann,† J. B. Lando,*,† L. Zhou,‡ and K. D. Singer‡

Departments of Macromolecular Science and Physics, Case Western Reserve University, Cleveland, Ohio 44106

Received May 7, 1993; Revised Manuscript Received August 31, 1993•

ABSTRACT: Side-chain liquid crystalline copolymers containing nitrobiphenyl were used to fabricate polar Langmuir multilayers. (Methoxyethoxy)methoxy terminal groups were incorporated in the copolymers to enhance the spreadability and monolayer formation of the copolymers. X-ray diffraction, second harmonic measurements, and pyroelectric studies all support the existence of a noncentrosymmetric structure for the polymeric multilayers. Thus, the possibility of using polymeric monolayers to prevent molecular turnaround upon X-type horizontal deposition was demonstrated. The molecular susceptibility for nitrobiphenyl was measured to be $(9.8 \pm 1.0) \times 10^{-30}$ esu. The linear relationship between the square root of the second harmonic intensity (pp) and the number of layers (see Schemes I–V) indicates the good quality of the multilayers. The copolymeric multilayers with shorter spacers (see Schemes I–V) were found to have a lower second harmonic response. An unusual pyroelectric response was observed for Cop11 multilayers. The pyroelectric coefficients were determined to be 2.85×10^{-10} C cm^{-2} °C^{-1} for Cop11 and 2.0×10^{-10} C cm^{-2} °C^{-1} for Cop4. FTIR–RA studies show that the aromatic rings of Cop4 and Cop11 multilayers stay oriented in liquid crystalline phases.

1. Introduction

A Langmuir monolayer can be transferred onto a substrate by three possible deposition types: X, Y, and Z. Each deposition type can be performed by immersing (or emersing) a substrate either perpendicular to the water surface (vertical deposition) or parallel to the water surface (horizontal deposition). Figure 1 shows the vertical version of deposition types. Only films deposited in the X or Z mode have the natural potential for a noncentrosymmetric structure. A noncentrosymmetric structure is essential for a material to be able to possess a $\chi^{(2)}$ nonlinear optical effect, pyroelectricity, and piezoelectricity. Unfortunately, Y-type deposition usually occurs. In addition, X- or Z-type deposition usually leads to a Y-type structure[1–4] because of molecular turnaround.[5,6] So far, only a few materials have been reported to produce genuine X- or Z-type multilayers.[4,7–10] From the tendency for amphiphiles to pack in a Y-type structure it can be deduced that the Y-type mode is usually the most stable form, since the interactions between adjacent monolayers are either hydrophobic–hydrophobic or hydrophilic–hydrophilic.

Since it is difficult to construct a polar film from a single material, two approaches have been adopted to solve the problem. The first one is to work with the natural tendency of the molecules to associate head groups in adjacent layers.[11–23] In this approach, two kinds of monolayers are used. One monolayer (A) is transferred in immersion and the other (B) in emersion mode. Thus, a stable ABAB, Y-type film is obtained. But with no plane of symmetry (noncentrosymmetric), since each bilayer consists of two different types of molecules (see Figure 2). In the second approach, a polymeric monolayer is used and deposited by X-type or Z-type. The use of polymer could prevent the molecules from turning around, if one considers the steric hindrance generated when polymers try to rearrange. The possibility was first demonstrated by Enkelmann and Lando.[10]

In this research, side-chain liquid crystalline polymers were used. Nitrobiphenyl ether was used as the active chromophore and attached to poly(methylsiloxane) through methylene units ($-(CH_2)_n-$, n = 4 or 11). Nitrobiphenyl chromophores were used to provide polarity for pyroelectricity and second-order nonlinear optical response. Nitro groups connected with delocalized π electrons can be expected to have high second-order molecular polarizability.[24] (Methoxyethoxy)methoxy was incorporated to enhance the spreadability of the polymers. The structure of the multilayers was examined by X-ray diffraction, second harmonic generation, and pyroelectric response. The molecular orientation and thermal transitions were investigated by FTIR–RA.

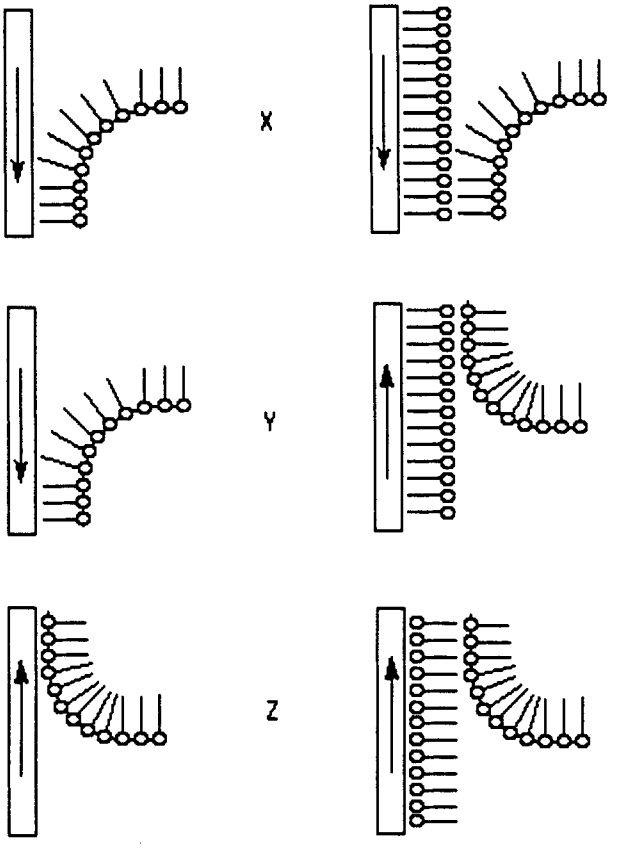

Figure 1. Possible deposition types: X, Y, and Z.

† Department of Macromolecular Science.
‡ Department of Physics.
• Abstract published in *Advance ACS Abstracts*, November 15, 1993.

0024-9297/93/2226-7263$04.00/0

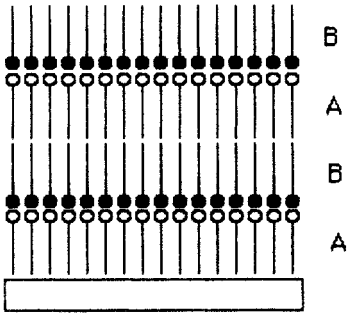

Figure 2. Y-type ABAB LB multilayer film.

2. Experimental Section

Synthesis. Materials. 10-Undecen-1-ol (99%), *p*-toluenesulfonyl chloride (99%), 4,4′-dihydroxybiphenyl (97%), 4-hydroxybiphenyl (97%), benzoyl chloride (99%), fumic nitric acid (90%), dimethyl sulfate (99%), 4-bromo-1-butene (99%), and (2-methoxyethoxy)methoxy chloride (MEMCl) were obtained from Aldrich and used as received.

For hydrosilation, toluene was washed with H_2SO_4 until the portions were relatively uncolored, washed with water until neutral pH, dried over $MgSO_4$, filtered, allowed to reflux overnight with Na metal, and then distilled from Na metal. The platinum divinyltetramethyldisiloxane catalyst (solution in xylene from Petrarch) was purified by placing it in a clean flamed-dried flask with a gas inlet adapter which was attached to a vacuum line under vacuum at 40 °C for 8 h, after which the remaining catalyst was diluted to 30 times its original volume with dried toluene.[25] Poly(hydrogenmethylsiloxane) (DP = 36) was generously supplied by J. Heck.

Techniques. ^{1}H-NMR (200-MHz) spectra were recorded on a Varian XL-200 spectrometer. Tetramethylsilane (TMS) was used as an internal standard. Melting points were obtained with a Thomas Hoover capillary melting point apparatus unless otherwise specified. Molecular weights were determined by gel permeation chromatography (GPC) with a Perkin-Elmer Series LC-10 instrument, equipped with an LC-100 column oven, and a Nelson Analytical integrator data station with a 900 series interface. The measurements were made at 40 °C, using $CHCl_3$ as solvent, with a UV detector (254 nm). A calibration plot constructed with polystyrene standards was used to determine the molecular weight. High-pressure liquid chromatography (HPLC) experiments were performed with the same instrument. A Du Pont thermal analyst 2000 equipped with a DSC standard data analysis program was used to obtain thermal behavior. Heating and cooling rates were 15 °C/min in all cases.

The synthesis is outlined in Schemes I–V.

Potassium 4-hydroxy-4′-nitrobiphenyl was synthesized according to a literature method[26] with some modification. The procedures are described in the following.

4-(Benzoyloxy)biphenyl (I). To a reaction mixture of 30 g (0.1763 mol) of 4-hydroxybiphenyl, 31.9 mL (0.2292 mol) of dry triethylamine (distilled from KOH), and 360 mL of dry THF (distilled from $LiAlH_4$) was added 22.5 mL (0.1938 mol) of benzoyl chloride at 0 °C, and the reaction mixture was stirred for 4 h at room temperature. The reaction mixture was then filtered. The liquids (THF and triethylamine) were evaporated. The resulting solid was washed with H_2O and hot methanol and recrystallized from *n*-butanol to yield 46.7 g (97%) of white crystals. Mp: 149–150 °C.

4-(Benzoyloxy)-4′-nitrobiphenyl (II). A total of 20 g (0.073 mol) of **I** was mixed with 160 mL of glacial acetic acid and heated to 85 °C. Fuming nitric acid (48 mL) was slowly added such that the temperature was kept between 85 and 90 °C, and the reaction mixture was stirred for another 30 min. The reaction mixture was filtered while hot. The resulting solid was washed with H_2O and methanol and recrystallized from glacial acetic acid to yield 10.5 g (45.1%) of light yellow crystals. Mp: 211–214 °C. ^{1}H-NMR ($CDCl_3$, TMS): δ 7.39 (d, 2H, ortho to –OOC), 7.57 (m, 3H, 2H, meta to –COO; 1H, para to –COO), 7.71 (d, 2H, meta to –OOC), 7.76 (d, 2H, meta to $-NO_2$), 8.24 (d, 2H, ortho to –COO), 8.32 (d, 2H, ortho to $-NO_2$).

Scheme I

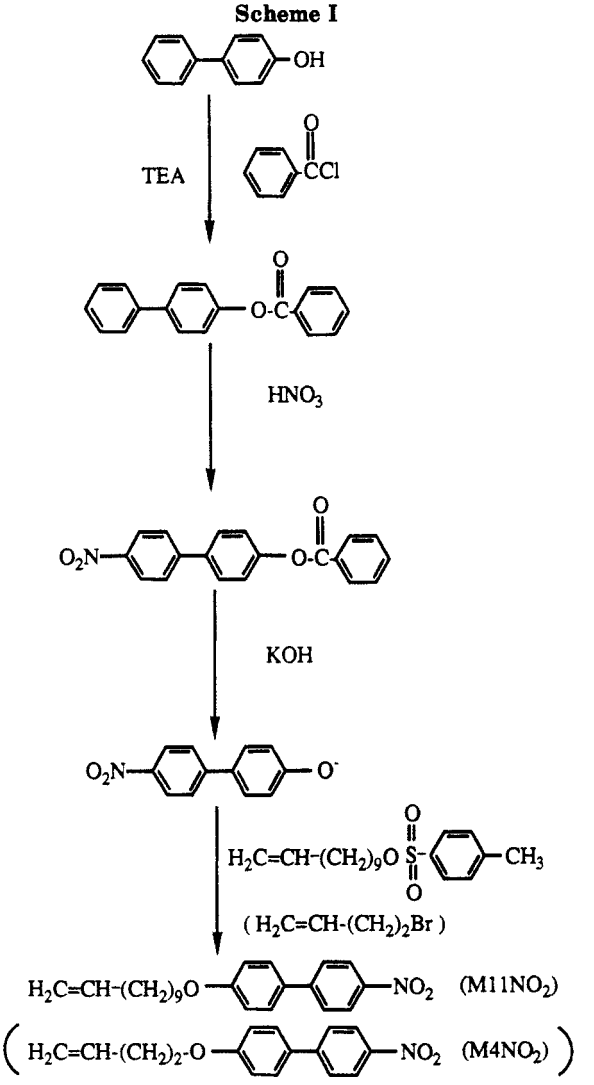

Scheme II

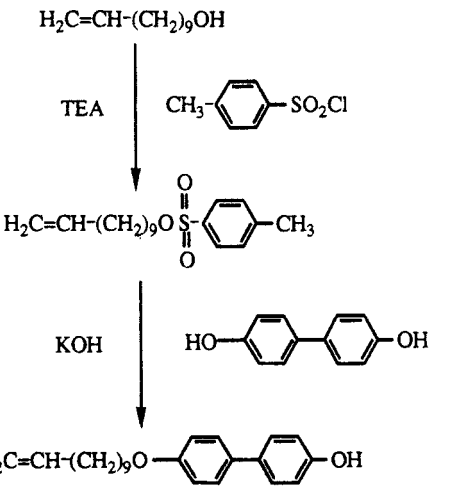

Potassium 4-Hydroxy-4′-nitrobiphenyl (III). A total of 10 g (31.3 mmol) of **II** was mixed with 60 mL of ethanol and heated to reflux. A solution of 6 g of KOH in 20 mL of water was added dropwise at reflux. The reaction mixture was refluxed for 30 min and then cooled overnight. The resulting purple crystals were filtered and washed with THF to yield 8.3 g (98.6%) of **III**. The salt was utilized in subsequent reactions. 4-Hydroxy-4′-nitrobiphenyl can be obtained by dissolving the salt in water and adding 50/50 HCl/H_2O. The yellow solid was filtered, washed with water, and recrystallized from ethanol. Mp: 203–204 °C. Purity: >99% (HPLC). ^{1}H-NMR (acetone-d_6, TMS): δ 6.99 (d,

Scheme III

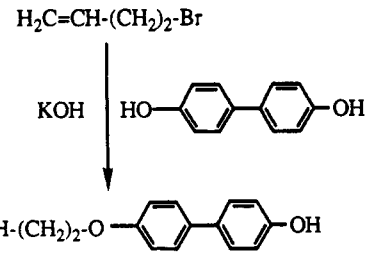

Scheme IV

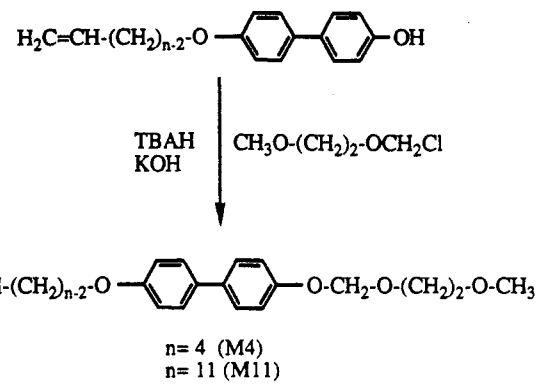

Scheme V

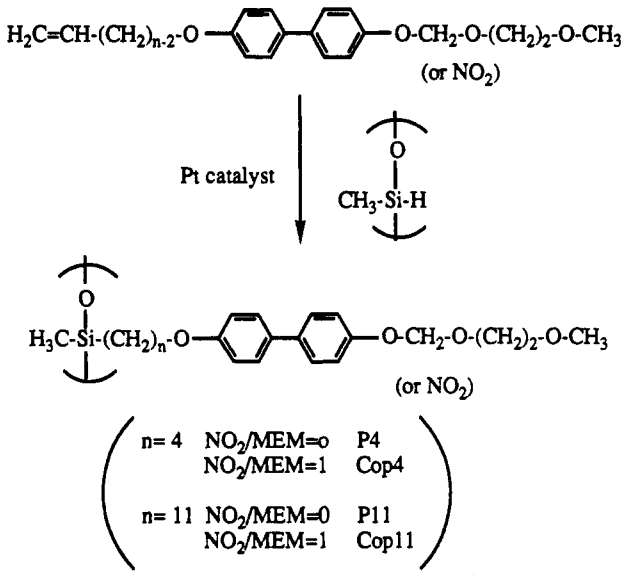

2H, ortho to –OH), 7.67 (d, 2H, meta to –OH), 7.88 (d, 2H, meta to $-NO_2$), 8.29 (d, 2H, ortho to $-NO_2$).

4-(10-Undecen-1-yloxy)-4′-nitrobiphenyl (M11NO₂). A reaction mixture containing 4 g (14.9 mmol) of **III**, 6.3 g (19.4 mmol) of 10-undecen-1-yl tosylate, 100 mL of ethanol, and 18 mL of H_2O was stirred at 80 °C for 6 h. The solid was filtered and recrystallized from methanol to yield 4.6 g (84.1%) of yellow crystals. Purity: >99% (HPLC). Mp: 69–70 °C. ^{1}H-NMR ($CDCl_3$, TMS): δ 1.32 (m, 12H, $-(CH_2)_6-$), 1.81 (m, 2H, $-CH_2CH_2OAr-$), 2.03 (m, 2H, $-CH_2CH{=}CH_2$), 4.01 (t, 2H, $-CH_2OAr-$), 4.94 (m, 2H, $CH_2{=}CH-$), 5.80 (m, 1H, $-CH{=}CH_2$), 6.99 (d, 2H, ArH ortho to alkoxy), 7.63 (d, 2H, ArH meta to alkoxy), 7.72 (d, 2H, ArH meta to $-NO_2$), 8.30 (d, 2H, ArH ortho to $-NO_2$).

4-(3-Buten-1-yloxy)-4′-nitrobiphenyl (M4NO₂). A reaction mixture containing 4 g (14.9 mmol) of **III**, 2.4 g (17.8 mmol) of 4-bromo-1-butene, 100 mL of ethanol, and 20 mL of water was refluxed for 12 h and cooled overnight. The yellow solid was filtered and recrystallized from water to yield 2.4 g (59.5%) of yellow crystals. Purity: >99% (HPLC). Mp: 67–68 °C. ^{1}H-NMR ($CDCl_3$, TMS): δ 2.56 (m, 2H, $-CH_2CH{=}CH_2$), 4.08 (t, 2H, $-CH_2OAr-$), 5.15 (m, 2H, $CH_2{=}CH-$), 5.91 (m, 1H, $-CH{=}CH_2$), 7.00 (d, 2H, ArH ortho to alkoxy), 7.55 (d, 2H, ArH meta to alkoxy), 7.69 (d, 2H, ArH meta to $-NO_2$), 8.26 (d, 2H, ArH ortho to $-NO_2$).

Table I. Molecular Weight and Molecular Weight Distribution of P4, Cop4, P11, and Cop11

monomer feed	polymer	$10^3 M_n$	M_w/M_n
M4	P4	21.4	3.4
M4/M4NO₂ (1/1)	Cop4	14.9	2.3
M11	P11	26.1	2.4
M11/M11NO₂ (1/1)	Cop11	19.2	2.1

The synthesis of 4-(10-undecen-1-yloxy)-4′-hydroxybiphenyl was performed according to a literature method.[27] Purity: >99% (HPLC). ^{1}H-NMR ($CDCl_3$, TMS): δ 1.30 (m, 12H, $-(CH_2)_6-$), 1.80 (m, 2H, $-CH_2CH_2OAr-$), 2.02 (m, 2H, $-CH_2CH{=}CH_2$), 4.00 (t, 2H, $-CH_2OAr-$), 4.98 (m, 2H, $CH_2{=}CH_2-$), 6.98–6.99 (m, 4H, ArH ortho to –O–), 7.42–7.50 (m, 4H, ArH meta to –O–).

4-(3-Buten-1-yloxy)-4′-hydroxybiphenyl (IV). A reaction mixture containing 20 g (0.107 mol) of 4,4′-dihydroxybiphenyl, 6.6 g (0.118 mol) of KOH, and 200 mL of methanol was refluxed for 1 h. To the resulting solution was added 15.9 g (0.118 mol) of 4-bromo-1-butene, and the reaction mixture was refluxed for 12 h. The solvent was then evaporated. The product was extracted by CH_2Cl_2, and CH_2Cl_2 was then evaporated. The resulting solid was washed with 10% KOH, filtered, and recrystallized from ethanol/water (1/1) to yield 7.5 g (29.2%) of white crystals. Purity: >99% (HPLC). Mp: 156–157 °C. ^{1}H-NMR ($CDCl_3$, TMS): δ 2.55 (m, 2H, $-CH_2CH{=}CH_2$), 4.06 (t, 2H, $-CH_2OAr-$), 5.13 (m, 2H, $CH_2{=}CH-$), 5.91 (m, 1H, $-CH{=}CH_2$), 6.86 (d, 2H, ArH ortho to –OH), 6.97 (d, 2H, ArH ortho to alkoxy), 7.30–7.58 (m, 4H, ArH meta to –O–).

4-(3-Buten-1-yloxy)-4′-[(methoxyethoxy)methoxy]biphenyl (M4). To a reaction mixture containing 4 g (16.7 mmol) of compound **IV**, 1.13 g (3.3 mmol) of tetrabutylammonium hydrogen sulfate (TBAH), 45 mL of THF, 15 g of KOH, and 15 g of H_2O was added 4.2 g (33.7 mmol) of MEMCl. The reaction mixture was stirred for 1 h. The product was extracted by THF, and then THF was evaporated. The solid was dissolved in $CHCl_3$ and washed with H_2O a couple of times. $CHCl_3$ was removed, and the resulting solid was washed with methanol and recrystallized from methanol to yield 4 g (73%) of white solids. Purity: >99% (HPLC). Mp: 61 °C (DSC, 15 °C/min). ^{1}H-NMR ($CDCl_3$, TMS): δ 2.56 (m, 2H, $-CH_2CH{=}CH_2$), 3.37 (s, 3H, CH_3O-), 3.59 (t, 2H, $-CH_2OCH_3$), 3.82 (t, 2H, $-CH_2CH_2OCH_3$), 4.04 (t, 2H, $-CH_2CH_2OAr$), 5.14 (m, 2H, $CH_2{=}CH-$), 5.29 (s, 2H, $-OCH_2OAr-$), 5.92 (m, 1H, $-CH{=}CH_2$), 6.94 (d, 2H, ArH ortho to alkoxy), 7.11 (d, 2H, ArH ortho to $-OCH_2O-$), 7.45 (d, 4H, ArH meta to –O–).

4-(10-Undecen-1-yloxy)-4′-[(methoxyethoxy)methoxy]biphenyl (M11). The synthesis is the same as compound M4. The yield was 83.9%. Purity: >99% (HPLC). Mp: 75 °C (DSC, 15 °C/min). ^{1}H-NMR ($CDCl_3$, TMS): δ 1.30 (m, 12H, $-(CH_2)_6-$), 1.79 (m, 2H, $-CH_2CH_2OAr-$), 2.02 (m, 2H, $-CH_2CH{=}CH_2$), 3.38 (s, 3H, CH_3O-), 3.58 (m, 2H, $-CH_2OCH_3$), 3.83 (m, 2H, $-CH_2CH_2OCH_3$), 3.99 (t, 2H, $-CH_2CH_2OAr-$), 4.95 (overlapped doublet, 2H, $CH_2{=}CH-$), 5.29 (s, 2H, $-OCH_2OAr$), 5.79 (m, 1H, $-CH{=}CH_2$), 6.93 (d, 2H, ArH ortho to alkoxy), 7.14 (d, 2H, ArH ortho to $-OCH_2O-$), 7.45 (d, 4H, ArH meta to –O–).

Hydrosilation. Hydrosilation was carried out according to a literature method.[25] An example of hydrosilation is given below. To a flame-dried 20-mL round-bottomed flask purged with nitrogen were added 1 g (2.35 mmol) of M4, 0.128 g (2.13 mmol) of poly(hydrogenmethylsiloxane), and 2–3 mL of dry toluene. The reaction mixture was heated to 60 °C, and 5 drops (about 0.1 g) of purified platinum divinyltetramethyldisiloxane catalyst was added. The reaction was followed by monitoring the Si–H stretching band at ~2152 cm^{-1}, using a dispersion IR instrument (Perkin–Elmer 1320). The Si–H band could not be detected after 2 h. The reaction mixture was stirred for another 2 h, then cooled, and precipitated into methanol. The precipitate was filtered, dissolved in chloroform, and reprecipitated into ethanol several times to remove catalyst and residual monomer. Four hydrosilations were performed. The results are presented in Table I. The compositions (NO_2/MEM) of Cop4 and Cop11 are close to 1 (the same as the feeding compositions) determined by NMR (see Figure 3). It was noticed that trace amounts of unreacted Si–H groups from Cop11 can still be detected by FTIR (see Figure 19).

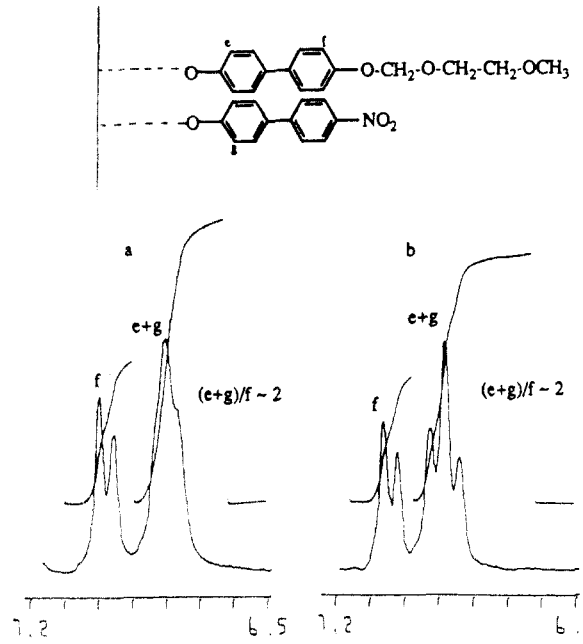

Figure 3. ^{1}H-NMR of (a) Cop4 and (b) Cop11.

Monolayer Characterization and Deposition. Monolayer manipulations were performed on a commercial Lauda film balance. This balance employs a floating Teflon barrier attached to a linear variable differential transducer to measure the differences in surface pressures between a clean water surface and that containing a film. The brass trough was coated with Teflon to prevent any metal ion impurities from leaching out of the trough. An IBM PC was interfaced with the film balance for data acquisition and processing. Software was developed for these purposes by Dr. J. D. Shutt.[28] All the isotherm collection and film deposition experiments were done in class 10 laminar flow areas inside a class 100 clean room. Subphase water was obtained from the ultrapurification of the local municipal water system using a Millipore water system. The system is comprised of a Milli-RO 120 and a Milli-Q plus to yield water with resistivity greater than 18.2 MΩ cm. Pretreatment of the municipal source consisted of an exchange carbon tank and a water softener. In addition, a single "shake test" is used to show the complete absence of any tendency to foam. This is a more sensitive test than the determination of surface tension which is always within the experimental uncertainty of the literature value. Capillary ripple damping is also checked as part of another experiment.

The spreading solutions had concentrations of 0.5–0.7 mg/mL in HPLC-grade $CHCl_3$. Initial spreading areas were greater than 80 Å^2/molecule, and dwell times of 10 min were used to ensure complete evaporation of the spreading solvent. Compression rates were 3.25 cm/min (the width of the trough is 15 cm). The water temperature was controlled by circulating thermostated water underneath the brass. The temperature of the water was measured by a surface probe to a precision of ±0.1 °C.

Vertical Deposition. The vertical deposition of monolayers onto substrates was achieved via a computer-controlled stepping motor. The motor has 3.9-μm steps, and the dipping speed was controlled by the pulse rates of the D/A outputs on the IBM PC. Speeds varying from 0.01 to 50 mm/min can be achieved.

Horizontal Deposition. A hydrophobic substrate was penetrated through a monolayer horizontally, which was first used by Day and Lando.[29] The residual monolayer was cleaned up, and then the substrate was withdrawn vertically to facilitate the draining of the water. It should be pointed out that the substrate penetrated through the monolayer horizontally with a small tilt angle to prevent air bubbles from being trapped inside.

Substrates. Multilayers were deposited on Corning microscope slides. The slides were degreased in a sequence, which is a standard procedure used for silicon wafers, as follows: 5 min of ultrasonic agitation in (1) trichloroethylene, (2) acetone, and (3) methanol, respectively. To obtain hydrophobic substrates, the degreased slides were then exposed to hexamethyldisilazane (HMDS) vapor in a glass desiccator for at least 48 h.

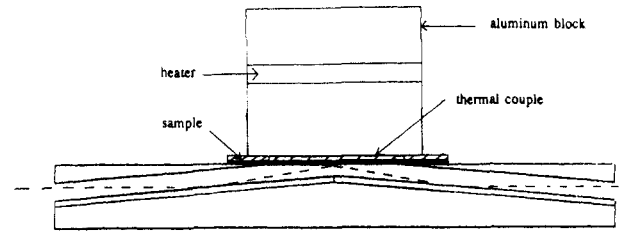

Figure 4. Schematic of the arrangement of the RA attachment, multilayer sample, and thermal control block used in the variable-temperature spectroscopic studies.

X-ray Diffraction. X-ray diffraction patterns were obtained using a Philips diffractometer with Cu Kα radiation. The multilayers deposited on microscope slides were examined.

Second Harmonic Generation (SHG). A Q-switched Nd:YAG laser was employed as a light source operated at 1064-nm output for the second harmonic measurement. The multilayers were deposited by X-type horizontal deposition.

Pyroelectricity. The pyroelectric device consists of a multilayer film sandwiched between two orthogonal rectangular aluminum strips (vacuum deposited) with a working area of 1 mm^2 defined by the width of the aluminum strip squared. The electrode patterns were applied onto hydrophilic glass substrates, using aluminum shadow masks. The substrates with bottom electrodes were rinsed with chloroform and then made hydrophobic by storing in HMDS vapor for at least 48 h. The thickness of the bottom electrode is 2000 Å, and that of the top electrode is 500 Å. The deposition rate was 500 Å/min. The deposition rate is most important for the top electrode, since a fast deposition could result in the damage of the deposited films.

Contacts to the electrode surfaces of the device were made using gold wire probes mounted on a Wentworth Lab probing station. The entire station was enclosed in an aluminum box to reduce air currents and electronic interference. A Keithly Model 616 digital electrometer was operated in the Coulomb mode in order to evaluate the change in charge with temperature. The samples were placed on the heating stage of the probing station. The stage was heated electrically and cooled with circulating water/methanol (−10 °C). The heating rate was 0.58 °C/s and the cooling rate was 0.35 °C/s between 18 and 40 °C. The measurements were carried out under ambient conditions with T = 20 °C and a relative humidity of 67%.

Optical Microscopy. A Carl-Zeiss optical polarizing microscope equipped with a Mettler FP 82 hot stage and a Mettler 800 central processor was used to observe the anisotropic textures.

FTIR: Transmission and Reflection Absorption (RA). Transmission and reflection spectra were acquired using a single-beam Digilab (Division of BioRad) FTS-60 Fourier transform infrared spectrometer equipped with a liquid-nitrogen-cooled mercury-cadmium-telluride (MCT) photoelectric detector. The FTS-80 RAS attachment supplied by Spectra Tech Technologies consisted of two rectangular gold mirrors inclined at an angle of 5° off horizontal. The substrate to be studied was placed horizontally above the peak of the two mirrors such that the incident radiation was reflected off the substrate at an incident angle of 80°.

Variable-temperature studies were performed between 25 and 165 °C using an aluminum block (1.5 × 2.25 × 1.875 in.) heated by a cartridge heater ($^3/_8$ × 2 in. $D \times L$). The temperature was controlled by a Digi-Sense temperature controller Model 2168–70, using a J-type sensor, which was attached to the edge of the aluminum block. The RAS attachment/sample/heater block assembly was placed within the sample chamber of the spectrometer as shown in Figure 4. Multilayers were prepared on aluminum-coated (vapor-deposited, 3000 Å) glass slides by X-type horizontal deposition. The aluminum-coated slides were exposed to hexamethyldisilazane (HMDS) vapor in a glass desiccator for at least 48 h prior to the deposition.

3. Results and Discussion

3.1. Monolayer Formation and Transfer Behavior.

Monomers M4NO$_2$ and M11NO$_2$ formed aggregates at the air/water interface upon spreading, indicating insufficient

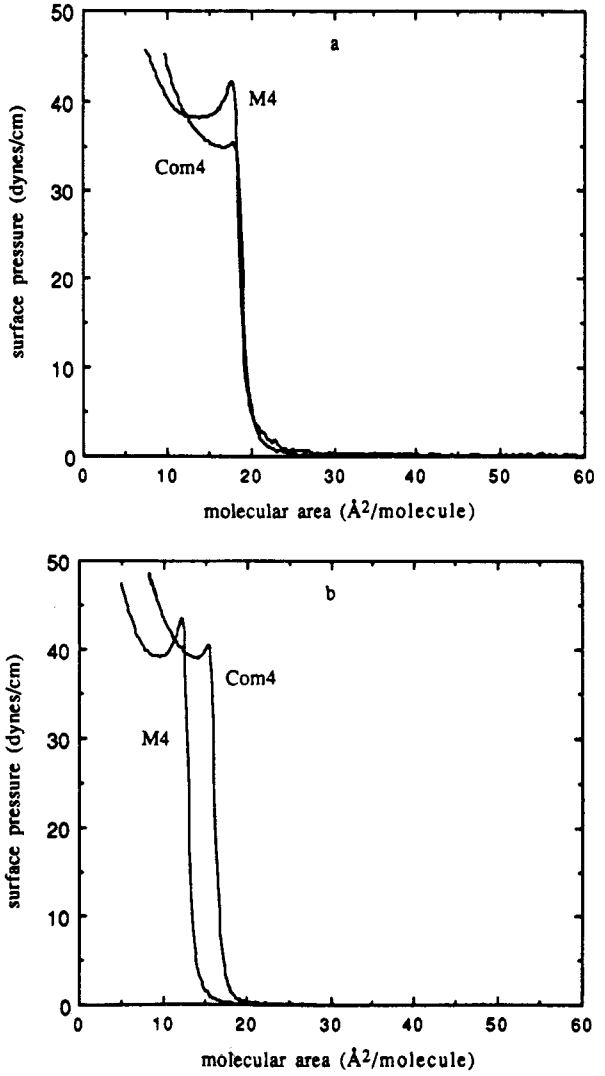

Figure 5. Surface pressure–molecular area isotherms of M4 and Com4 (NO_2/MEM = 1) with dwell times of (a) 10 min and (b) 1 h before compression.

hydrophilicity of nitro groups. In order to enhance the spreadability and monolayer formation, a mixed-monolayer concept was adopted. The concept was first employed by Xu et al.[30,31] They succeeded in forming a good monolayer by mixing 4-nitro-4′-(octadecyloxy)azobenzene with 4-carboxy-4′-(octadecyloxy)azobenzene. In this research, (methoxyethoxy)methoxy groups were incorporated to provide hydrophilicity. Figure 5a shows the surface pressure–molecular area (π–A) isotherms of monomers M4 and Com4 (M4 mixed with M4NO_2, 1/1 ratio). The molecular areas of the isotherms at the condensed phase were somewhat low (the cross-sectional area of planar biphenyl was calculated to be 22.9 Å² [32], which suggests either a three-dimensional structure or dissolution of the molecules. To identify the cause, the isotherms were collected (see Figure 5b), using a dwell time of 1 h before compression. The results show that longer dwell times resulted in more dissolution and thus a much lower apparent molecular area of the condensed phase. Figure 6 shows the π–A isotherms of monomers M11 and Com11 (M11 mixed with M11NO_2, 1/1 ratio). The isotherms show that the monomers with longer spacers formed good monolayers, since the solubility was reduced. In addition, the mixed monolayer (Com11) formed a more condensed packing than M11. Figures 7 and 8 show the π–A isotherms of P4 and Cop4 and of P11 and Cop11, respectively. Compared with monomers M4 and Com4, the use of polymers (P4 and Cop4) decreases the solubility and

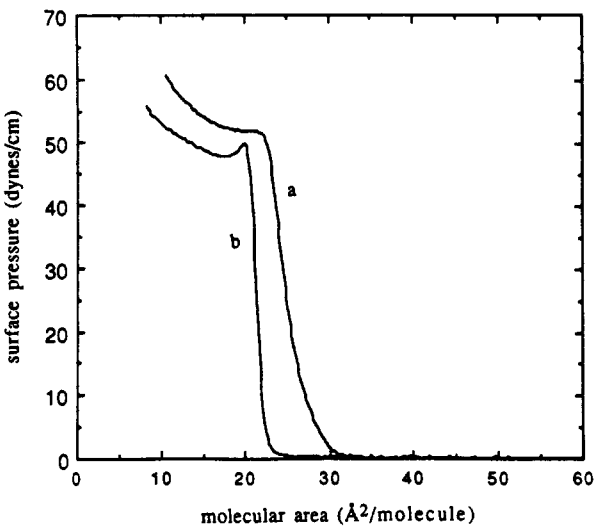

Figure 6. Surface pressure–molecular area isotherms of (a) M11 and (b) Com11 (NO_2/MEM = 1).

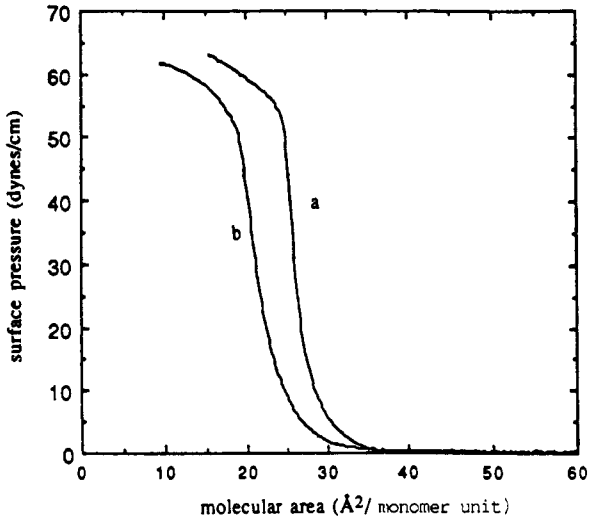

Figure 7. Surface pressure–molecular area isotherms of (a) P4 and (b) Cop4.

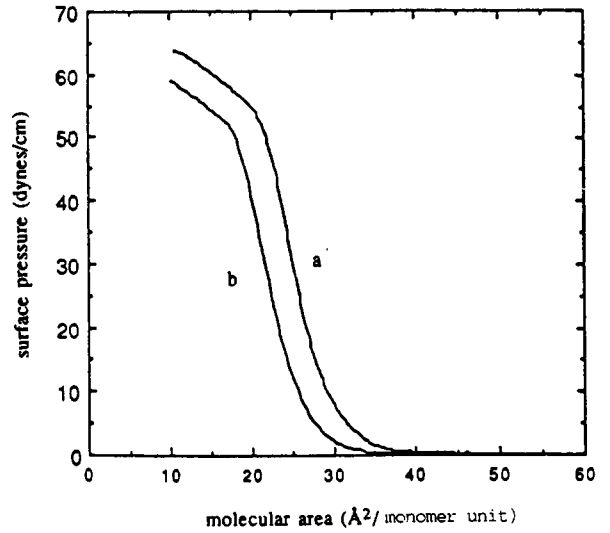

Figure 8. Surface pressure–molecular area isotherms of (a) P11 and (b) Cop11.

enables the formation of stable monolayers. Copolymeric monolayers show a more condensed packing than homopolymers, which is consistent with the results from monomeric monolayers.

The transfer of the monolayers onto substrates was initially tested by vertical deposition. M11 showed Z-type

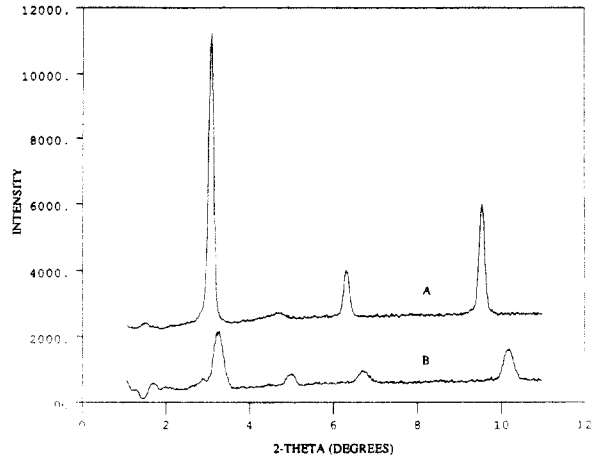

Figure 9. X-ray diffraction traces of 10-layer M11 films by (a) X-type horizontal deposition and (b) Z-type vertical deposition.

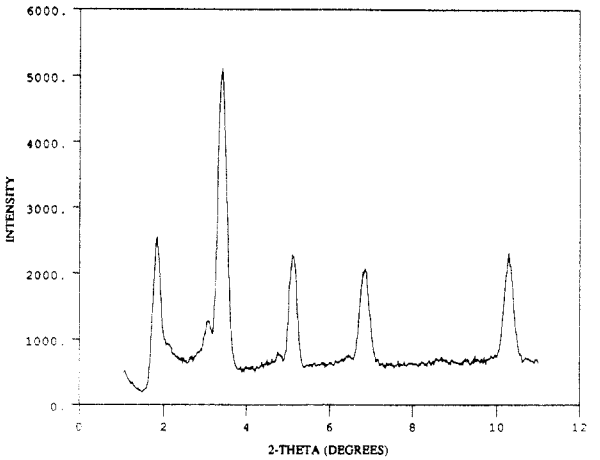

Figure 10. X-ray diffraction trace of a 10-layer Com11 (NO_2/MEM = 1) film by X-type horizontal deposition.

deposition. The attempts to transfer polymeric monolayers by vertical deposition were not successful, probably because of the high viscosity of the polymeric monolayers. The general features were (1) Z-type deposition, (2) the transfer ratio was not reproducible, and (3) the transfer became more and more difficult as the deposition went on. Therefore, X-type horizontal deposition was employed.

3.2. X-ray Diffraction. Since the molecules are highly oriented in a direction normal to the substrate, an X-ray diffraction trace of the multilayers could provide information about the periodicity of the structure in that direction. Comparing d_{001} with the calculated fully-extended chain length, one should be able to infer if the molecular repeat is one molecule (noncentrosymmetric) or two molecules (centrosymmetric).

Figure 9 shows X-ray diffraction traces of M11 by vertical deposition and by horizontal deposition. Two peaks appear on the vertically deposited sample at 2θ 1.73° (d = 51 Å) and 4.80° (d = 18 Å), corresponding to 001 and 003 reflections from a centrosymmetric structure if one considers the fully-extended chain length of 27.9 Å determined by SYBYL modeling. On the other hand, only a trace 003 peak can be detected on the horizontally deposited sample. It suggests that the molecules can turn around more easily by vertical deposition than by horizontal deposition. Figure 10 shows the X-ray diffraction trace of Com11 as a reference, the two peaks at 2θ = 1.87° (d = 47.2 Å) and 5.15° (d = 17.2 Å) correspond to 001 and 003 reflections, indicating a centrosymmetric structure. Figure 11 shows X-ray diffraction traces of P4, Cop4, P11,

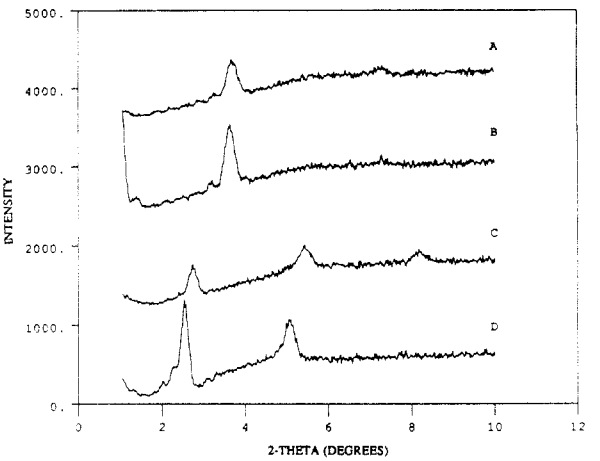

Figure 11. X-ray diffraction traces of 10-layer films (A) P4, (B) Cop4, (C) P11, and (D) Cop11 by X-type horizontal deposition.

Table II. d-Spacing (001) from X-ray Diffraction and Fully-Extended Chain Length by SYBYL Modeling

multilayers	d_{001} (Å) from X-ray	fully-extended chain length (Å) by SYBYL
P4	24.0	26.1
Cop4	24.5	26.1
P11	32.4	35.1
Cop11	35.0	35.1

and Cop11. Table II lists the values of d_{001}s calculated from X-ray diffraction and the fully-extended chain length by SYBYL modeling. It can be seen that d_{001}s are smaller or comparable to the fully-extended chain lengths, suggesting noncentrosymmetric structures in all cases. The significance of these results is that it is possible to use polymer to prevent molecular turnaround and maintain an unnatural noncentrosymmetric structure. It was noticed that Cop11 multilayers appeared to have a perpendicular orientation with respect to the substrate. This will be compared to the result from second harmonic measurements.

3.3. Nonlinear Optics. Second harmonic generation (SHG) is a process in which light with a frequency ω interacts with a polar medium and is partially converted into light with a frequency of 2ω. Instead of a specific molecular excitation, this process arises from the residual noncentrosymmetric second-order polarizability. Therefore, SHG is a sensitive probe of acentric structures. In this study, second harmonic generation was measured to determine the nonlinear optical properties as well as the film structure. This technique for determining the film structure is well-known and based on the relationship between symmetry, order, and the nonlinear optical susceptibility.[33-36] Assuming rotational symmetry about the film normal and about the molecular long axis, the two nonzero susceptibility components with respect to the film plane are

$$\chi^{(2)} = N\beta^*_{zzz}\langle\cos^3\theta\rangle \quad (1)$$

$$\chi^{(2)} = (1/2)N\beta^*_{zzz}\langle\cos\theta\sin^2\theta\rangle \quad (2)$$

where N is the number density, β the molecular nonlinear optical susceptibility, z the direction of the long axis of the nitrobiphenyl, and θ the angle between the film normal and the molecular z axis. We use the usual assumption of a δ-function distribution to determine the tilt angle from the second harmonic generation experiments.[33] The two susceptibilities given in eqs 1 and 2 can be measured with two polarization schemes, and the tilt angles, determined from them.[35,36] The number density can be

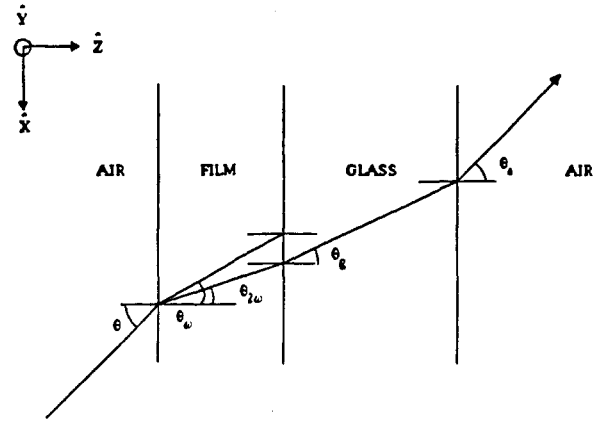

Figure 12. Sample geometry for second harmonic generation measurements.

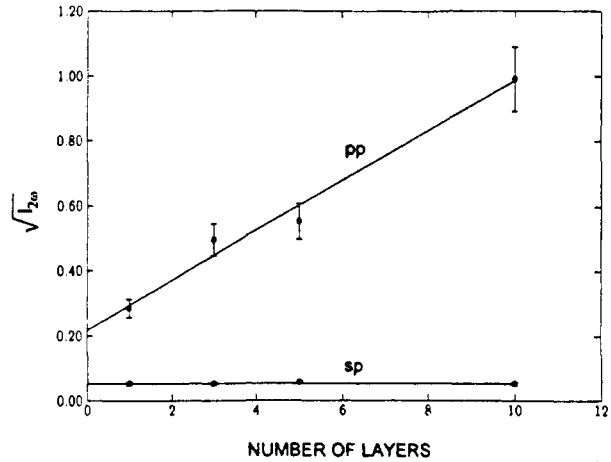

Figure 13. Square root of the second harmonic intensities as a function of the number of layers.

determined from the area of the spread monolayer, the number of layers, and the layer thickness so that β^*_{zzz} can be determined.

Copl1 multilayers were first measured. The experimental geometry is shown in Figure 12, where p-polarized light has its electric field vector lying in the plane of incidence and s-polarized light has its electric field vector perpendicular to the plane of incidence. The two experiments to determine the two susceptibilities correspond to p-polarized second harmonic light with either the p-polarized fundamental (pp) or the s-polarized fundamental (sp). The other two polarizations ss and the ps are not allowed in this symmetry group. The intensities of the p-polarized or s-polarized fundamental and p-polarized second harmonic light were measured by scanning the incident angle between the propagation direction and the surface normal. Both pp and sp measurements exhibit maxima at −68 and +68° with zero signal at 0° which indicates an azimuthally symmetric distribution about the film normal. Symmetry about the film normal (lack of inplane order) was verified by our inability to detect an ss- and ps-polarized signal. The intensity of the pp signal is related to a linear combination of $\chi^{(2)}$ and $\chi^{(2)}$, while the sp intensity is proportional to $\chi^{(2)}$. Thus, these two measurements determine θ, β, and $\chi^{(2)}$.

The square root of the second harmonic intensities as a function of the number of layers is shown in Figure 13. The linearity of the pp intensity as a function of the number of layers confirms the polar head-to-tail structure determined from X-ray diffraction. The constant value of the sp intensity as a function of the number of layers suggests that only the first layer contributes to this signal. As θ

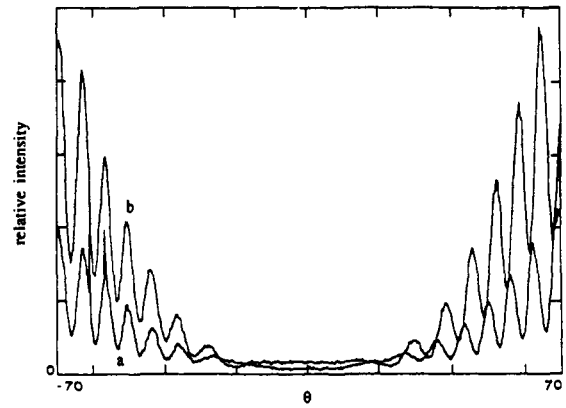

Figure 14. Second harmonic generation (pp) of 10-layer films (a) Cop4 and (b) Copl1 at variable incident angles.

decreases, the magnitude of $\chi^{(2)}$ decreases, and likewise the sp intensity decreases; both are zero at $\theta = 0°$. This suggests the first layer is tilted much more than subsequent layers, and these subsequent layers are nearly perpendicular to the film plane, which is consistent with the X-ray diffraction result and the nonzero intercept of the pp intensities. Since both susceptibility components contribute to the pp intensity, it should be larger for larger tilt angle. Thus, the first layer has a tilt angle of about $22 \pm 2°$, while the subsequent layers have a nearly constant and small or zero tilt angle.

The second harmonic coefficient $d = \chi^{(2)}/2$ is $(5.3 \pm 0.5) \times 10^{-9}$ esu. The molecular susceptibility is $(9.8 \pm 1.0) \times 10^{-30}$ esu which is in agreement with the result of Cheng and co-workers on EFISH (electric-field-induced second harmonic generation) measurements on similar chromophores when dispersion is taken into account.[37] The susceptibility calculations agreed within a few percent for the monolayer and multilayer films with the orientations as given above. This confirms the conclusions regarding the differing structure of the first and subsequent layers. All measurements were found to be reproducible over the span of several weeks, indicating a stable structure.

Figure 14 shows the second harmonic generation of 10-layer films of Cop4 and Copl1. The fringes result from the interference of the glass substrates. The X-ray diffraction result indicates that Cop4 multilayers have a slight tilt angle. The second harmonic intensity is expected to increase with tilt angle up to about 40°. Since the observed tilt angle is less than 40°, the observed lower intensity may indicate a more disordered alignment of Cop4 multilayers and possibly some molecular rearrangement during deposition which was not detected by X-ray diffraction studies. It is possible that the copolymer with a longer spacer (Copl1) might have a more restricted side-chain motion, which makes the molecular rearrangement more difficult.

3.4. Pyroelectricity. Both X-ray and nonlinear optical studies have supported the existence of noncentrosymmetric structures for Copl1 multilayers and, to some extent, Cop4 multilayers. Therefore, possible pyroelectric devices can be made out of these multilayer films.

The pyroelectric measurements were performed on 10-multilayer films of Copl1, Cop4, P11, and P4. P11 and P4 samples were used to verify the stability of the instrument and identify the source of pyroelectric response. No response could be detected on samples P11 and P4 between 18 and 35 °C. Therefore, any response generated from samples Copl1 and Cop4 must be attributed to nitrobiphenyl groups.

The pyroelectric response of the Copl1 sample was measured from 19 to 35 °C. It showed an unusual

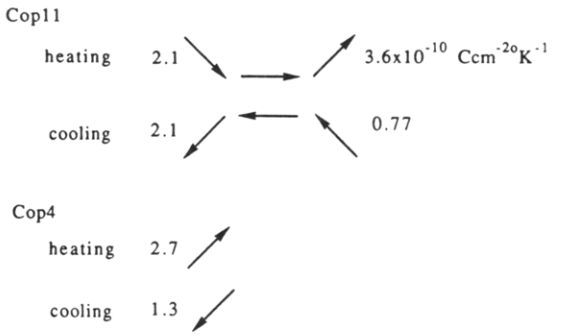

Figure 15. Pyroelectric response of Cop11 and Cop4 multilayers.

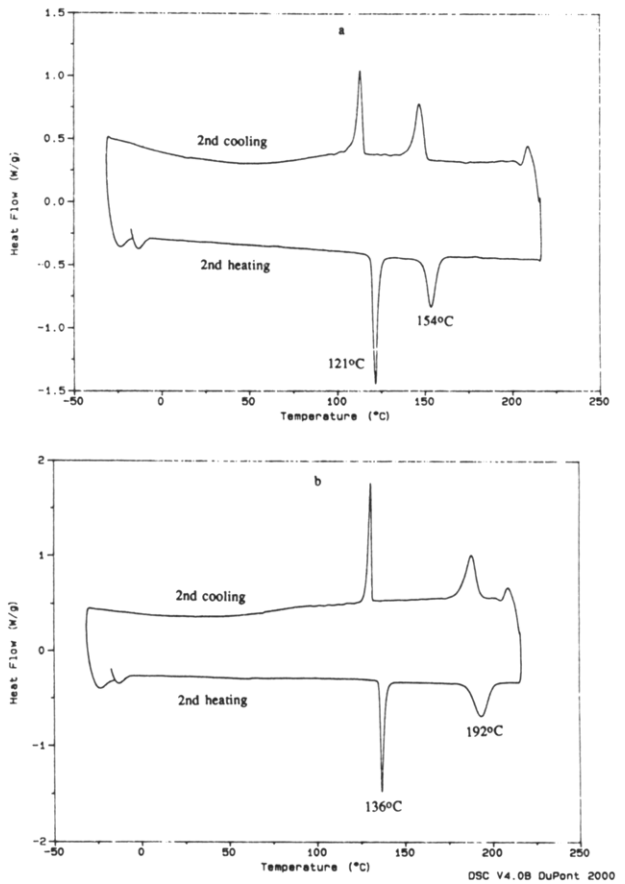

Figure 16. DSC traces of bulk samples (a) Cop4 and (b) Cop11 (second heating and second cooling).

characteristic (see Figure 15). Upon heating, there was an average decrease in charge accumulation of 2.1×10^{-10} C cm^{-2} °C^{-1} from 19 to 22 °C, the charge stayed almost constant between 23 and 27 °C, and then there was an average increase of 3.6×10^{-10} C cm^{-2} °C^{-1} between 28 and 33 °C. Upon cooling, there was an increase in charge accumulation of 0.77×10^{-10} C cm^{-2} °C^{-1} between 33 and 28 °C, the charge stayed constant between 27 and 23 °C, and then there was a decrease of 2.10×10^{-10} C cm^{-2} °C^{-1} in charge accumulation between 22 and 19 °C. The whole process was reversible, and the same pattern was detected after 2 months and with other similarly prepared multilayers.

Initially, a transition state was assumed. Therefore, the measurements were performed, starting from 22, 25, 27, and 30 °C, respectively. The response still shows the same pattern, indicating the assumption was not correct. There are a number of possible explanations of these data. At present we are attempting to elucidate the reason or reasons for this behavior, which will be the subject of a future paper. It should be noted that no evidence for a

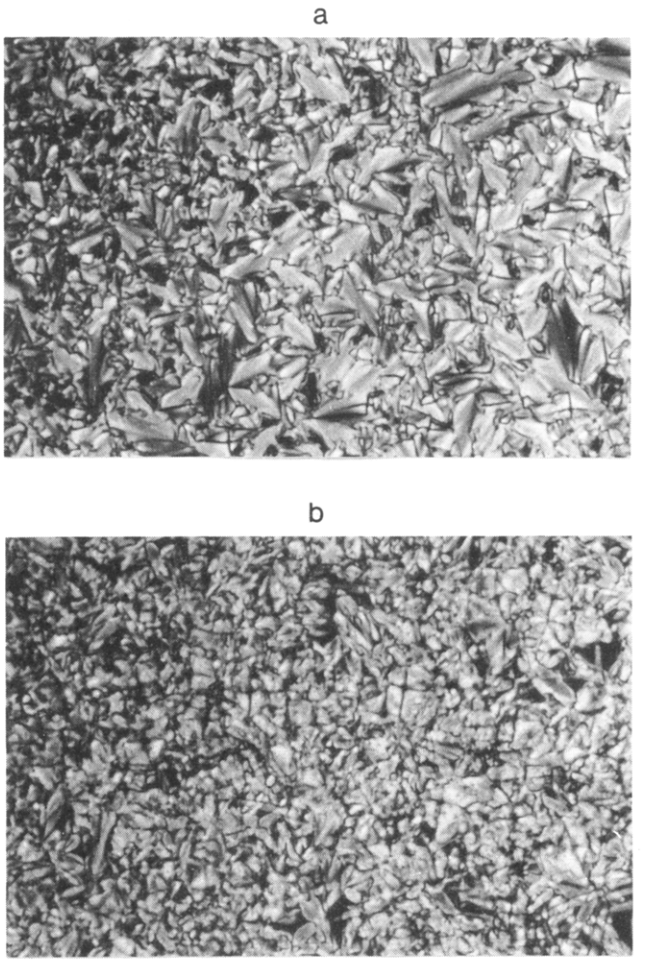

Figure 17. Polarized optical micrographs of (a) Cop4 at 150 °C and (b) Cop11 at 186 °C.

reorientation of dipoles in this temperature range has been observed by spectroscopic means.

The pyroelectric response of Cop4 was measured between 20 and 30 °C, and there was an increase in charge accumulation of 2.7×10^{-10} C cm^{-2} °C^{-1} upon heating and a decrease in charge accumulation of 1.3×10^{-10} C cm^{-2} °C^{-1} upon cooling (see Figure 15). It seems that the usual factors, thermal expansion and thermal libration, are operative in this case.

Averaging the pyroelectric coefficients for heating and cooling gives 2.85×10^{-10} C cm^{-2} °C^{-1} for Cop11 and 2.0×10^{-10} C cm^{-2} °C^{-1} for Cop4. The values are somewhat higher than those of some acid–amine alternating-layer systems reported in the literature.[12-17]

3.5. Molecular Orientation and Thermal Transition by FTIR–Reflection Absorption (RA). Both Cop4 and Cop11 bulk samples show smectic liquid crystalline phases from DSC (see Figure 16) and polarized optical microscope (see Figure 17) studies. Therefore, FTIR–RA was employed to detect the molecular orientation of the multilayers with respect to temperature. Reflection absorption spectroscopy is a very useful technique that gives information about the direction of transition dipoles in a sample.[38] In general, the parallel components of incident and reflected rays interfere to produce a standing-wave electric field which is perpendicular to the substrate. On the other hand, the electric field vector, **E**, is parallel to the substrate in transmission measurements. A combination of these two techniques can provide information about the orientation of the molecules.

Figure 18 and 19 show the FTIR–RA and transmission spectra of Cop4 and Cop11, respectively. RA spectra were

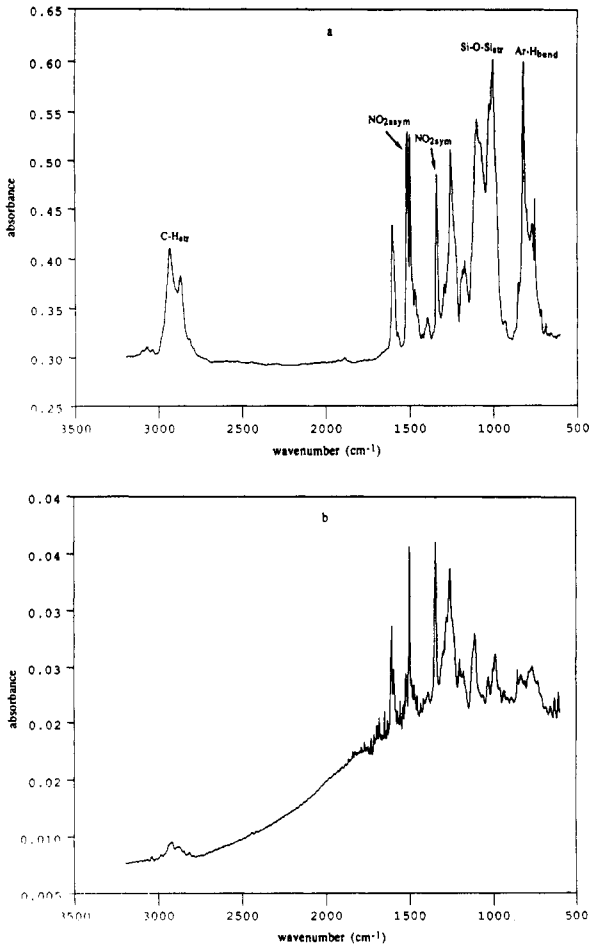

Figure 18. IR spectra of Cop4 by (a) the transmission method, using a powder KBr pellet sample, and (b) the RA method, using a 10-layer sample.

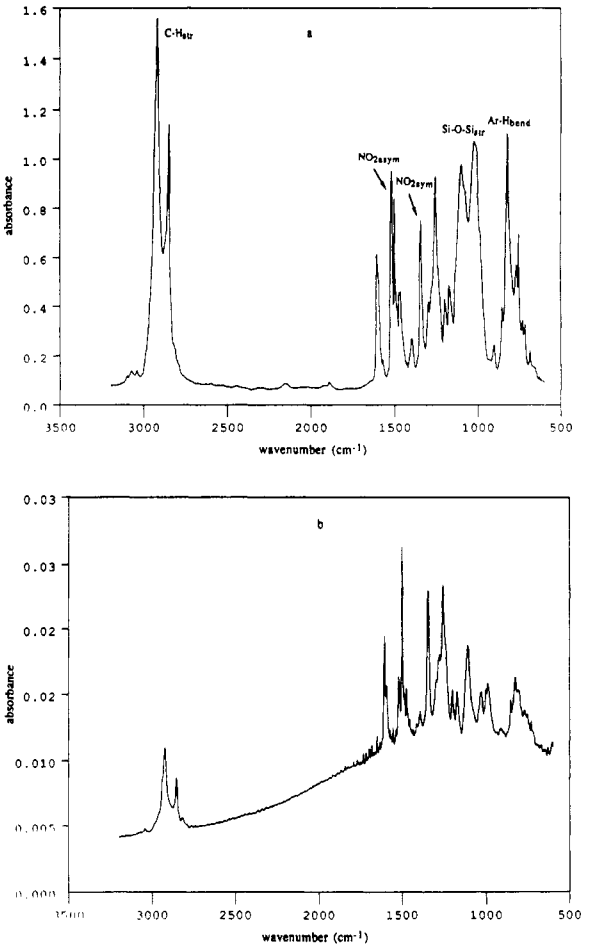

Figure 19. IR spectra of Cop11 by (a) the transmission method, using a powder KBr pellet sample, and (b) the RA method, using a 10-layer sample.

taken from 10-layer films. Transmission spectra were taken as references, using powder KBr pellets which can be assumed to be isotropic. Because of the complexity of the spectra, only the bands, which are easy to identify and sensitive to the molecular orientation, will be discussed.

C–H Stretching Region from 2800 to 3000 cm^{-1}. Both $-CH_3$ and $-CH_2-$ groups contribute to this region.[39,40] CH_2 asymmetric and symmetric stretching bands are the most useful for the determination of orientation. For an aliphatic chain in an all-trans planar zigzag conformation oriented normal to the substrate surface, both the symmetric and asymmetric stretches lie parallel to the plane of the substrate. Therefore, the methylene stretching will not be picked up by a perpendicular electric field in the RA technique.[41] The significant decrease of the relative intensity around this region by RA indicates that alkyl chains and MEM chains were aligned more or less perpendicular to the substrate. It was noticed that, although X-ray diffraction suggests an almost perpendicular orientation of Cop11, significant CH_2 stretching bands can still be detected by RA, indicating a disordered packing to some extent.

Si–O–Si Stretching Region from 1000 to 1100 cm^{-1}. Besides the two strong and broad Si–O–Si bands near 1020 and 1090 cm^{-1}, there are some other bands showing up at this region, which are probably due to C–O stretching of Ar–O–C and C–O–C and aromatic C–H in-plane bending.[39,40] The substantial decrease on the relative intensity around this region in the RA spectra indicates that siloxane backbones were oriented more or less parallel to the substrate.

C–H Out-of-Plane Bending of Para-Substituted Aromatics at 822 cm^{-1}. This region is complicated by the additional contribution from NO_2 scissors deformation at ~859 cm^{-1} and NO_2 out-of-plane wagging at ~756 cm^{-1}.[39,40] Nevertheless, the band still serves as a good guidance on the orientation of aromatic rings due to the sharpness of the band. It can be seen in Figures 18 and 19 that the sharp C–H out-of-plane bending at 822 cm^{-1} can hardly be detected in the RA spectra. This is a good indication that the aromatic rings are oriented almost perpendicular to the substrate.

NO_2 Asymmetric Stretching at 1518 cm^{-1} and Symmetric Stretching at 1345 cm^{-1}. The relative intensity of the asymmetric to symmetric NO_2 stretching vibration modes in the RA spectra and the transmission spectra reflected the fact that the dipole moment of symmetric NO_2 stretching was oriented more or less perpendicular to the substrate.

With the preceding discussion as a basis, the variations in molecular orientation with respect to temperature can now be pursued. In the following discussion, variable-temperature RA spectra will be presented. The absorbance of the C–H stretching region will be plotted against temperature to identify small changes.

For sample Cop4, there appears to be a premelting process and two transition states, one at 115–125 °C and the other at 155–165 °C from examining the absorbance of the C–H stretching region (see Figure 20). For the second transition, significant changes were also detected in the Si–O–Si stretching region and the aromatic C–H out-of-plane bending (see Figure 21). The premelting

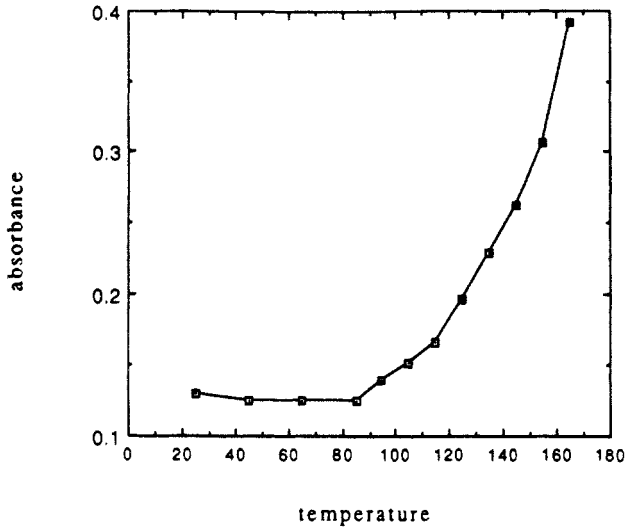

Figure 20. Absorbance of the C–H stretching region versus temperature or a 10-layer Cop4 sample.

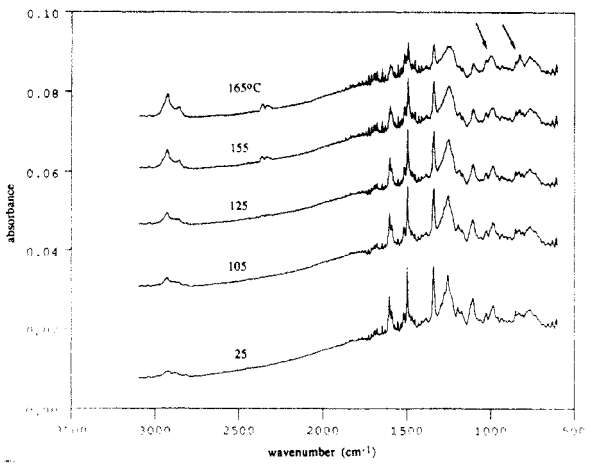

Figure 21. Variable-temperature RA spectra of a 10-layer Cop4 sample.

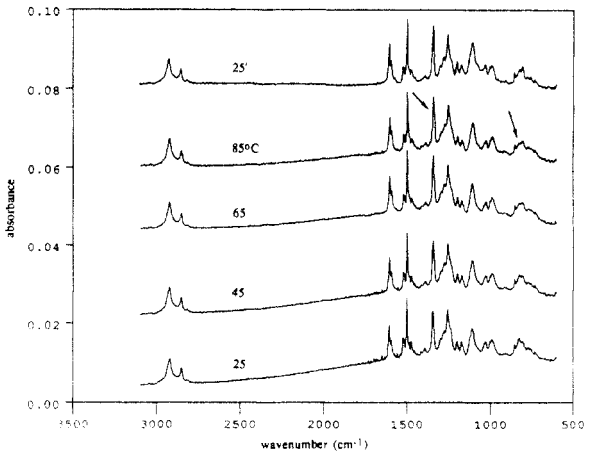

Figure 22. Variable-temperature RA spectra of a 10-layer Cop11 sample from 25 to 85 °C.

process probably indicates some disordered packing in the film.

Sample Cop11 showed an annealing effect. Figure 22 shows that the intensity of the aromatic C–H out-of-plane bending decreases and the intensity of the NO_2 symmetric stretching band increases from 25 to 85 °C, indicating a more perpendicular direction of nitrobiphenyl groups. The same sample was cooled to 25 °C and scanned again. The spectrum (see Figure 22, 25 °C) suggests that the process was not reversible. It was felt that the phenomenon might

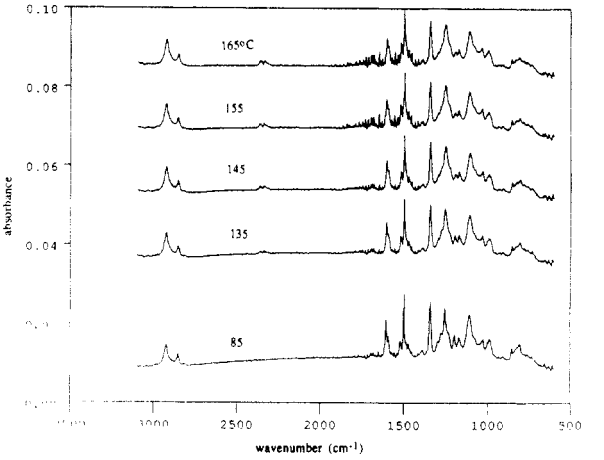

Figure 23. Variable-temperature RA spectra of a 10-layer Cop11 sample from 85 to 165 °C.

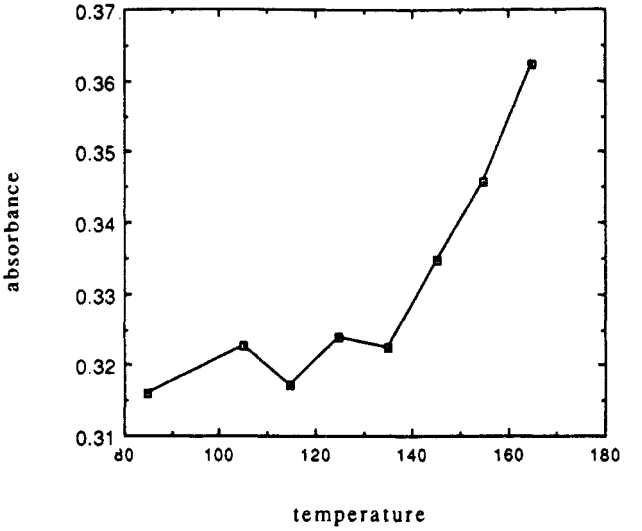

Figure 24. Absorbance of the C–H stretching region versus temperature for a 10-layer Cop11 sample.

Table III. Thermal Transition by FTIR–RA (Multilayers) and DSC (Bulk Samples)

	thermal transition (°C)	
material	FTIR–RA	DSC (2nd heating)[a]
Cop4	115–125	121 (c–lc)
	155–165	154 (lc–i)
Cop11	135–145	136 (c–lc)
		192 (lc–i)

[a] c, crystal; lc, liquid crystal; i, isotropic.

also indicate the restricted motion of the side chain with longer spacer as described in the sections of nonlinear optics and pyroelectricity, since it was only observed on the polymers with longer spacer (Cop11) rather than the ones with shorter spacer (Cop4). Some metastable packings appeared to be frozen in due to the restriction. The same sample was examined from 85 to 165 °C. Figure 23 shows the spectra. The intensity of the C–H stretching region was plotted against temperature (see Figure 24). There appears to be a small transition between 135 and 145 °C.

Comparing the transitions from FTIR–RA with the results from DSC (see Table III), it appears that the small transition determined from RA corresponds to crystal–liquid crystal transition and the large transition corresponds to liquid crystal–isotropic transition. It is interesting to see that the aromatic rings of the molecules (Cop4 and Cop11) seem to be able to stay oriented at the liquid

crystalline phases since no significant change on the aromatic C–H out-of-plane bending was detected.

4. Conclusions

Monomers M4NO_2 and M11NO_2 formed aggregates at the air/water interface upon spreading due to insufficient hydrophilicity. The incorporation of (methoxyethoxy)-methoxy facilitates the spreadability and monolayer formation. However, the formation of monomeric monolayers was affected by water solubility, especially for the one with shorter spacer (M4). The solubility effect can be minimized by the use of a longer spacer or by making the groups side chains on a polymer. The π–A isotherms suggest the formation of good monolayers for polymers P11, Copl1, P4, and Cop4.

It is difficult to transfer polymeric monolayers by vertical deposition. Therefore, horizontal deposition was performed. X-ray diffraction, second harmonic measurements, and pyroelectric studies all support the existence of a noncentrosymmetric structure for polymeric multilayers. Second harmonic measurements and pyroelectric studies also show the good stability of Copl1 multilayers. Thus, the possibility of using polymeric monolayers to prevent molecular turnaround upon X-type horizontal deposition and maintain an unnatural noncentrosymmetric structure was demonstrated.

The molecular susceptibility for nitrobiphenyl was measured to be $(9.8 \pm 1.0) \times 10^{-30}$ esu. The linear relationship between the square root of second harmonic intensity and the number of layers for Copl1 suggests the good quality of the films. The copolymeric multilayers with shorter spacers (Cop4) was found to have a lower second harmonic response.

An unusual pyroelectric response was observed for Copl1 multilayers. The pyroelectric coefficients were determined to be 2.85×10^{-10} C cm^{-2} °C^{-1} for Copl1 and 2.0×10^{-10} C cm^{-2} °C^{-1} for Cop4.

FTIR–RA was employed to study the molecular orientation of Cop4 and Copl1 multilayers with respect to temperature. The aromatic rings of the multilayers appeared to stay oriented in liquid crystalline phases.

Acknowledgment. We gratefully acknowledge that this work was supported by the National Science Foundation under the Science and Technology Center ALCOM DMR89–20147.

References and Notes

(1) Momose, A.; Hirai, Y.; Waki, I.; Imazeki, S.; Temioka, Y.; Hayakawa, K.; Naito, M. *Thin Solid Films* **1989**, *178*, 519.
(2) Tregold, R. H.; Allen, R. A.; Hodge, P. *Thin Solid Films* **1987**, *155*, 343.
(3) Biddle, M. B. Ph.D. Dissertation, Case Western Reserve University, Cleveland, OH, 1988, Chapter 5.
(4) Fukuda, K.; Shiozawa, T. *Thin Solid Films* **1980**, *68*, 55.
(5) Langmuir, I. *Science* **1983**, *87*, 493.
(6) Honig, E. P. *J. Colloid Interface Sci.* **1973**, *43*, 66.
(7) Daniel, M. F.; Lettington, O. C.; Small, S. M. *Thin Solid Films* **1983**, *99*, 61.
(8) Blinov, L. M.; Dubinin, N. V.; Mikhnev, L. V.; Yudin, S. G. *Thin Solid Films* **1984**, *120*, 161.
(9) Popovitz-Biro, R.; Hill, K.; Sharit, E.; Hung, D. J.; Lahav, M.; Leiserowitz, L.; Sagiv, J.; Hsiung, H.; Meredith, G. R.; Vanherzeele, H. *J. Am. Chem. Soc.* **1990**, *112*, 2498.
(10) Enkelmann, V.; Lando, J. B. *J. Polym. Sci., Polym. Chem. Ed.* **1977**, *15*, 1843.
(11) Daniel, M. F.; Smith, G. W. *Mol. Cryst. Liq. Cryst.* **1984**, *102*, 193.
(12) Smith, G. W.; Daniel, M. F.; Barton, J. W.; Ratcliffe, N. *Thin Solid Films* **1985**, *132*, 125.
(13) Christie, P.; Roberts, G. G.; Petty, M. C. *Appl. Phys. Lett.* **1986**, *48*, 1101.
(14) Christie, P.; Jones, C. A.; Petty, M. C.; Roberts, G. G. *J. Phys. D: Appl. Phys.* **1986**, *19*, L167.
(15) Smith, G. W.; Evans, T. J. *Thin Solid Films* **1987**, *11*, 305.
(16) Smith, G. W.; Matcliffe, N.; Roser, Daniel, M. F. *Thin Solid Films* **1987**, *151*, 9.
(17) Jones, C. A.; Petty, M. C.; Roberts, G. G. *Thin Solid Films* **1988**, *159*, 461.
(18) See: Reference 3, p 222.
(19) Shih, K. S. Ph.D. Dissertation, Case Western Reverse University, Cleveland OH, 1988, p 219.
(20) Hermann, J. P.; Ducuing, J. *J. Appl. Phys.* **1974**, *45*, 5100.
(21) Daniel, M. F.; Smith, G. W. *Mol. Cryst. Liq. Cryst.* **1984**, *102*, 193.
(22) Oirling, I. R.; Kolinsky, P. V.; Cade, N. A.; Earls, J. D.; Peterson, I. R. *Opt. Commun.* **1985**, *55*, 289.
(23) Neal, D. B.; Petty, M. C.; Roberts, G. G.; Ahmad, M. M.; Feast, W. J.; Girling, I. R.; Cade, N. A.; Kolinsky, P. V.; Peterson, I. R. *Electron. Lett.* **1986**, *22*, 460.
(24) Oudar, J. L. *J. Chem. Phys.* **1977**, *67*, 446.
(25) Percec, V.; Heck, J. *Polym. Bull.* **1991**, *25*, 55.
(26) Leslie, T. M.; Demartino, R. N.; Choe, E. W.; Khanarian, G.; Hass, D.; Nelson, G.; Stamatoff, J. B.; Stuetz, D. E.; Teng, C.; Yoon, H. *Mol. Cryst. Liq. Cryst.* **1987**, *153*, 451.
(27) Percec, V.; Heck, J. *J. Polym. Sci. Polym. Chem. Ed.* **1991**, *29*, 591.
(28) Shutt, J. D. Ph.D. Dissertation, Case Western Reserve University, Cleveland, OH, 1988.
(29) Day, D.; Lando, J. B. *Macromolecules* **1980**, *13*, 1478.
(30) Era, M.; Tsutsui, T.; Saito, S. *Langmuir* **1989**, *5*, 1410.
(31) Xu, X.; Era, M.; Tsutsui, T.; Saito, S. *Thin Solid Films* **1989**, *178*, 541.
(32) Hargreaves, A.; Rizvi, S. H. *Acta Crystallogr.* **1962**, *15*, 365.
(33) Heinz, T. F.; Chen, C. K.; Richard, D.; Shen, Y. R. *Phys. Rev. Lett.* **1982**, *48*, 478.
(34) Heinz, T. F.; Tom, H. W. K.; Shen, Y. R. *Phys. Rev.* **1983**, *A28*, 1883.
(35) Kuzyk, M. G.; Singer, K. D.; Zahn, H. E.; King, L. A. *J. Opt. Soc. Am.* **1989**, *B6*, 742.
(36) LeGrange, J. D.; King, L. A.; Singer, K. D.; Katz, H. E.; Schilling, M. L. *J. Opt. Soc. Am.* **1989**, *B6*, 1946.
(37) Cheng, L. T.; Tam, W.; Feiring, A. *Proc. SPIE* **1990**, *1337*, 203.
(38) Ishida, H. *Rubber Chem. Technol.* **1987**, *60*, 497.
(39) Colthup, N. B.; Daly, L. H.; Wiberley, S. E. *Introduction to Infrared and Raman Spectroscopy*; Academic Press: San Diego, CA, 1990.
(40) Lin-Vien, D.; Colthup, N. B.; Fateley, W. G.; Grasselli, J. G. *The Handbook of Infrared and Raman Characteristic Frequencies of Organic Molecules*; Academic Press: San Diego, CA, 1991.
(41) Rabolt, J. F.; Burns, F. C.; Schlotter, N. E.; Swalen, J. D. *J. Chem. Phys.* **1983**, *78*, 946.